Skin health properties of *Paeonia lactiflora* flower extracts and tyrosinase inhibitors and free radical scavengers identified by HPLC post-column bioactivity assays

Huiji Zhou [a], Tingzhao Li [a,b], Bo Li [a,b,*], Shuai Sun [a,b,**]

[a] *Amway (Shanghai) Science and Technology Development Co., Ltd, Shanghai, 201203, Shanghai, China*
[b] *Amway (China) Botanical R&D Center, Wuxi, 214145, China*

A B S T R A C T

Skin health is a major concern across the world. The *Paeonia lactiflora* Pall. flower (PLPF) is well-known in China as an edible ornamental flower, that has been traditionally prescribed for the treatment of irregular menstruation and dysmenorrhea. However, its chemical constituents and bioactivities have not been systematically stuided. This study tentatively identified 27 compounds in aqueous and ethanol extracts of PLPF using ultra-performance liquid chromatography with quadrupole time-of-flight mass spectrometry, including four monoterpene glycosides, six phenols, six tannins, ten flavonoids and a hydroxycinnamic acid amide. Online antioxidant and tyrosinase inhibitor screening assays based on post-column bioactivity tests were used to screen for bioactive compounds in the extracts. Online and offline bioactivity assays showed that both extracts exhibited notable antioxidant properties against DPPH, ABTS, and FRAP, potent antiglycation capacity, and significant inhibition of tyrosinase, cyclooxygenase-2, and collagenase. Gallic acid derivatives were the main contributors to the antioxidant and antityrosinase capacity and may also inhibit cyclooxygenase-2 and collagenase, but they exhibited weak antiglycation capacity. The antiglycation effects may be due to the synergistic action of gallic acid and specific flavonoids. PLPF is a promising source of bioactive compounds for the development of natural skin health products.

1. Introduction

Excessive production of reactive oxygen species (ROS) is highly detrimental to skin health as it affects skin cell function, leading to inflammation, deep wrinkles, and loss of skin tone and resilience [1]. ROS can trigger complex inflammatory signal cascades such as aberrant cyclooxygensse-2 (COX-2) expression [2], and initiate the activation of enzymes that degrade extracellular matrix proteins in the dermis, such as collagen [3–5]. Wrinkling and sagging of skin result from the breakdown of collagen by collagenase [6]. Tyrosinase (TYR) is a multifunctional enzyme involved in melanogenesis. It is responsible for the hydroxylation of *L*-tyrosine to *L*-dopa and the oxidation of *L*-dopa to *O*-quinones, which are converted to melanin pigment deposits in the skin [7]. ROS also participate in glycation—a spontaneous nonenzymatic reaction between amino acid residues and reducing sugars that genarates advanced glycation
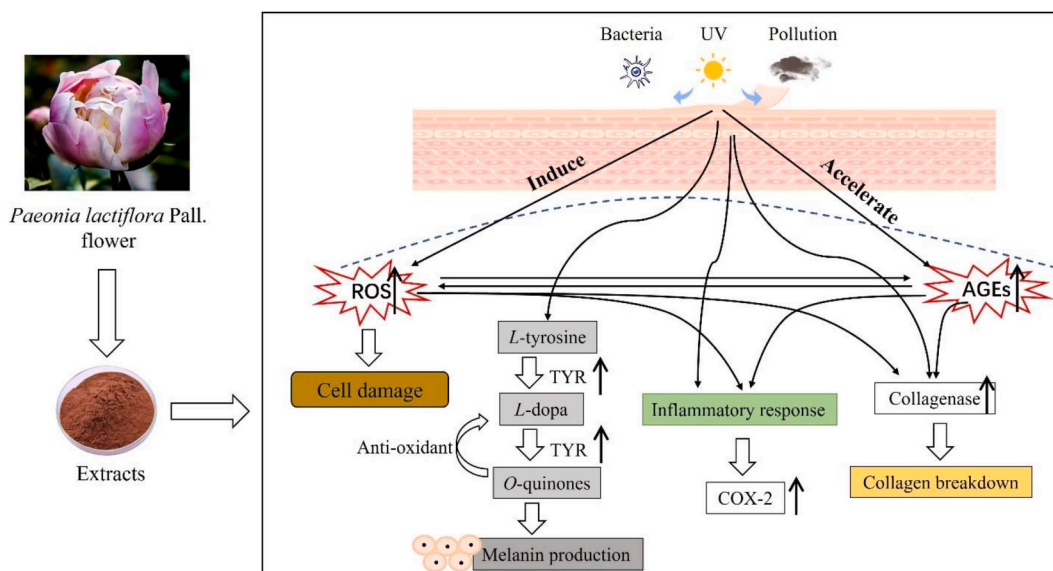

Fig. 1. Overview of the production of reactive oxygen species and advanced glycation end products and their effects on skin health.

end products (AGEs) [8,9]. Many studies have shown that irreversible AGEs generation is related to skin fibroblast damage [10], destruction of collagen fibers, and the dull, yellow skin complexion that can accompany aging [11–13]. The development of anti-oxidants and inhibitors of COX-2, collagenase, TYR, and glycation are crucial for addressing skin health problems (Fig. 1).

Paeonia lactiflora Pall. (PLP), which belongs to the Paeoniaceae family, is a well-known ornamental and medicinal plant with large, attractive flowers. It is common in China and Japan [14] and its dried roots have a long history in traditional Chinese medicine, with claims being made for its anti-inflammatory, antiviral, antibacterial, immune system modulating, cardioprotective and neph-roprotective properties [15–18]. However, the flowers of PLP (PLPF), which fall off naturally at the end of the ornamental period, can be considered as an untapped medicinal by-product because their chemical constituents and pharmacological effects have not been studied in detail. PLPF are safely eaten in China in common folk delicacies, such as flower tea, porridge, and wines [19].They are also often prescribed as traditional herbal medicines for treatment of irregular menstruation and dysmenorrhea [20]. Recent studies indicate that extracts of PLPF possess excellent antioxidant and tyrosinase inhibition properties [21–23]. Despite this, active com-pounds in PLPF and their effects on skin-related properties have been little studied. A better understanding of the biological activities of PLPF is needed to expand their use in functional foods and cosmetics.

Given the scarcity of scientific data concerning PLPF, this study investigated the composition of their aqueous and ethanol extracts. Twenty-seven compounds, including monoterpene glycosides, phenols, tannins and flavonoids, were tentatively identified using ultra-performance liquid chromatography coupled with photodiode array detection and quadrupole electrospray ionization time-of-flight mass spectrometry (UPLC-PDA-ESI-QTOF-MS/MS). Online antioxidant and anti-TYR post-column bioassay tests were applied to rapidly screen and identify the bioactive compounds in PLPF extracts. *In vitro* analysis of the major compounds was conducted to determine their potential biological impact on skin aging, specifically their antioxidant (DPPH, ABTS, FRAP), whitening (anti-TYR), antiglycation, COX-2 inhibiting, and anticollagenase properties.

2. Materials and methods

2.1. Plant materials and reagents

Paeonia lactiflora Pall. flowers were obtained from Bozhou County, Anhui Province, China and were authenticated by Dr. Xuefei Cai of Amway Botanical Research Center, China. Acetonitrile and acetic acid (HPLC grade) were obtained from Merck (Darmstadt, Ger-many). Reference standards of quinic acid, gallic acid, oxypaeoniflorin, methyl gallate, kaempferol-3,7-diglucoside, isorhamnetin-3,7-diglucoside, albiflorin, paeoniflorin, ethyl gallate, astragaloside, 1,2,3,6-tetra-*O*-galloy-β-D-glucopyranose, ellagic acid, isoquercitrin, 1,2,3,4,6-pentagalloyl glucose, isorhamnetin-3-*O*-glucoside, arbutin, rutin, and epigallocatechin gallate (EGCG) were obtained from Nature Standard Biotech Co. (China). Bovine serum albumin (BSA) lyophilized powder, 2,2′-azino-*bis*-3-ethylbenzothiazoline-6-sul-fonic acid (ABTS, 98%), 2,2-diphenyl-1-picrylhydrazyl radical (DPPH•, 98%), 6-hydroxyl-2,5,7,8-*tetra*-methylchroman-2-carboxylic acid (Trolox), tyrosinase, collagenase from *Clostridium histolyticum* (ChC) (≥125 CDU/mg solid), ascorbic acid, N-[3-(2-furyl)acryloyl]-Leu-Gly-Pro-Ala (FALGPA), and dimethyl sulfoxide (DMSO) were obtained from Sigma-Aldrich (Darmstadt, Germany). The FRAP kit (Ferric Reducing Ability of Plasma) and celecoxib (COX-2 inhibitor) were purchased from Beyotime Biotechnology Co. (Shanghai, China). All chemicals were of analytical or reagent grade and used without further purification. Ultrapure water was provided by a Milli-Q laboratory water purification system (Bedford, MA, USA).
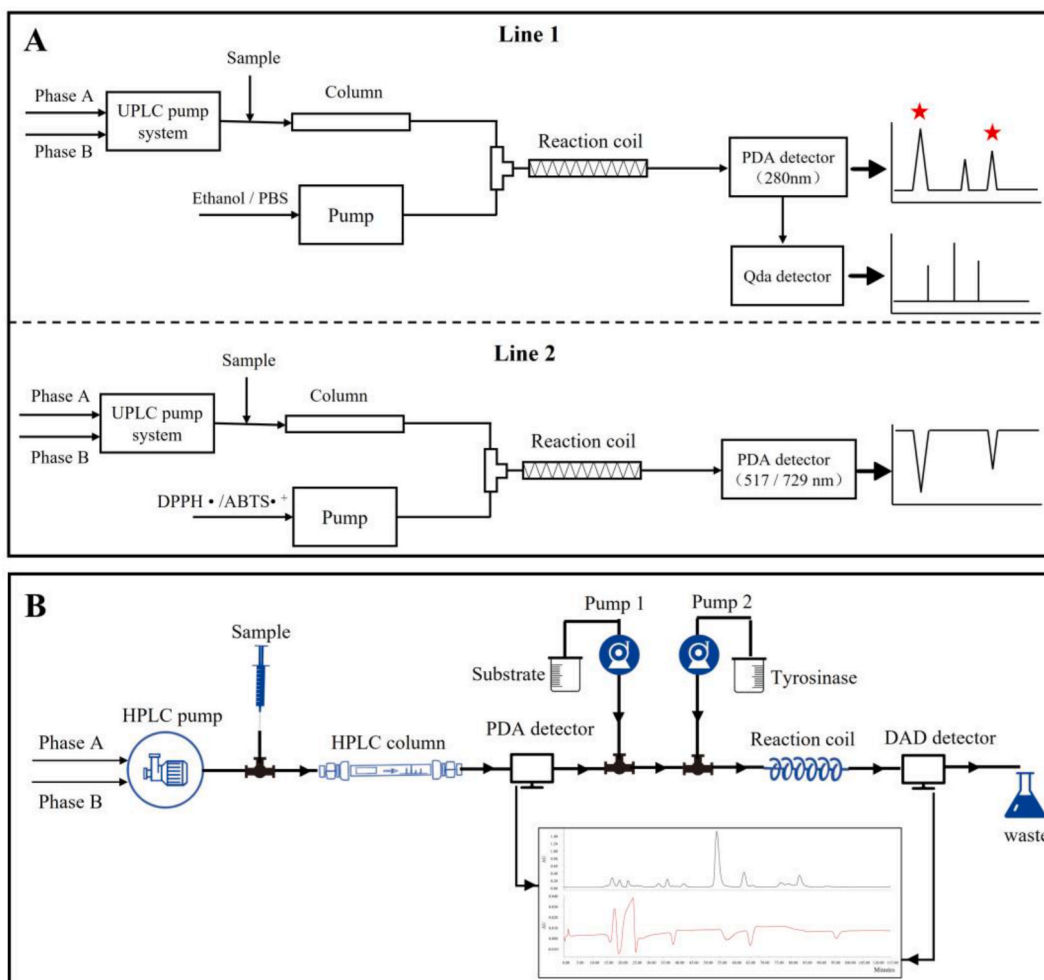
Fig. 2. Instrument setup for online screening of (A) DPPH and ABTS antioxidants by UPLC, and (B) Antityrosinase inhibitors by HPLC.

2.2. Extraction procedure

Pulverized flower powder (20 g) was ultrasonically extracted twice for 30 min at room temperature using 200 mL of ethanol/water (70/30, v/v) or ultrapure water. Following centrifugation at 19,000 g for 15 min at 4 °C (RWB3220CY-2, Eppendorf, Germany), the supernatant was concentrated at 50 °C under reduced pressure in a rotary evaporator (Hei-VAP Expert, Heidolph; Schwabach, Germany), then lyophilized to dryness in a freeze dryer. Water extracts were designated PLPF-W and ethanol/water extracts PLPF-E. Lyophilized powder was stored at −20 °C. PLPF-W residues were redissolved in ultrapure water and PLPF-E in 20% DMSO for subsequent bioassays.

2.3. UPLC-PDA-QTOF-ESI-MS/MS analysis

PLPF-W and PLPF-E residues were redissolved in ultrapure water and methanol, respectively, and passed through 0.45 μm syringe filters before analysis.

Mass spectrometry was performed on an Agilent 1290 UPLC system (Agilent, California, USA), including a sample manager and binary solvent manager, coupled to an Agilent Q-TOF 6545 MS system and PDA detector (scanning range 190–400 nm). An Acquity HSS T3 reverse phase column (2.1 mm × 100 mm, 1.8 μm; Waters, Milford, MA, USA) was used at 30 °C for chromatographic separation (1 μL sample injection volume). Mobile phases A (0.2% acetic acid in ultrapure water) and B (100% acetonitrile) at a flow rate of 0.2 mL/min were used for gradient elution as follows: 0–3 min, 95-90% A; 3–5 min, 0–85% A; 5–20 min, 85-80% A; 20–22 min, 80-50% A; 22–24 min, 50% A; 24–28 min, 50-20% A; 28–30 min, 20% A; 30–32 min, 20–95% A, and equilibrating at the initial conditions for 2 min. The column was equilibrated for an additional 2 min before each run. The MS was operated in both positive and negative ion modes under the following optimized conditions: TOF mass range, 50–1700 m/z; ion source gas, 50 psi; curtain gas, 35 psi; ion spray voltage, 5 kV; ion source temperature, 500 °C; and collision energy, 10 eV. Optimized MS/MS parameters were: mass range, 100–1500

m/z; collision energy, 40 eV; declustering potential, 100 V; and collision energy spread, 20eV. Analyte peaks were identified by comparing retention times, accurate masses, and formulas against external standards and commercial databases, and quantified using calibration curve peak areas at five concentrations.

2.4. Antioxidant capacity (DPPH•, ABTS•+ and FRAP assays)

Fast colorimetric methods were used for *in vitro* assessment of DPPH• scavenging [24], ABTS•$^+$ [25] decolorization, and FRAP total antioxidant capacity [26]. DPPH and ABTS stock solutions were prepared as previously described [27], and FRAP solution as per the FRAP kit. All measurements were carried out in triplicate and Trolox was used as a positive control.

DPPH• and ABTS•$^+$ radical scavenging activities were calculated as follows:

$$\% \text{ inhibition} = \left[\left(A_{control} - A_{sample} \right) \ / \ A_{control} \right] \times 100$$

where $A_{control}$ is the absorbance of the blank and A_{sample} is the absorbance of the test sample. The IC_{50} (the concentration of sample required for 50% radical inhibition) was calculated by plotting sample concentration against % inhibition.

For FRAP total antioxidant capacity, 0.15, 0.3, 0.6, 0.9, 1.2, and 1.5 mM $FeSO_4$ solutions were used for the calibration curve, with the FRAP value being represented by a $FeSO_4$ concentration. The regression equation of the curve was used to calculate equivalent concentration 1 (EC_1) for each sample. EC_1 is defined as the concentration of antioxidant giving an absorbance equivalent to that of 1.0 mM $FeSO_4$ determined using its own calibration curve [28].

2.5. Online antioxidant profiling using HPLC-PDA with post-column derivatization

Major antioxidant compounds in PLPF-W and PLPF-E were screened using online HPLC-DPPH and HPLC-ABTS post-column derivatization as previously described [29,30], with slight modifications. The phytochemicals were monitored in line A, with a second pump delivering ethanol or PBS to the PDA detector operating at 280 nm (Fig. 2A line 1). The antioxidant components were monitored in line B, with the second pump delivering DPPH radical or ABTS working solution to the detector, where decolorization of the mixture was detected photometrically as a negative peak at 517 nm (DPPH) or 729 nm (ABTS) (Fig. 2A line2). Separation of compounds (sample injection volume 2 μL) was achieved at 30 °C on a Kromasil 100-5-C_{18} column (4.6 mm × 250 mm, 5 μm; AkzoNobel, Sweden). Mobile phases A (0.2% acetic acid) and B (100% acetonitrile) at 0.7 mL/min were used for elution as follows: 0–5 min, 5–10% B; 5–8 min, 10–15% B; 8–40 min, 15–20% B; 40–55 min, 20% B; 55–60 min, 20–50% B; 60–65 min, 50–80% B; 65–70 min, 80% B; and 70–75 min, 80-5% B. DPPH and ABTS reagents were pumped into a 10 m reaction coil (0.25 mm ID) at 0.2 mL/min and 37 °C.

2.6. Antityrosinase assay

The antityrosinase activity of the samples was analyzed in 96-well microplates according to a previously described protocol [31,32] with minor changes: 0.5 mM L-tyrosine and 0.5 mM L-dopa were dissolved in 0.2 M phosphate buffer (PBS, pH 6.8), and mushroom tyrosinase (25 kU) was dissolved in 0.2 M phosphate buffer (500 mL, pH 6.8) in an ice bath to form tyrosinase stock solution (500 U/mL) and stored at −20 °C (then diluted with PBS before use).

Monophenolase inhibition was analyzed in a final volume of 200 μL. Initially, 50 μL of 0.5 mM L-tyrosine substrate, and 100 μL of sample or positive control solution were mixed and preincubated for 5 min at 37.5 °C before 50 μL of tyrosinase solution (250 U/mL) was added to initiate the reaction. The absorbance of the reaction mixture was measured at 475 nm after 15 min on a microplate reader (BioTek, USA).

Diphenolase inhibition was measured as follows: 50 μL of 0.5 mM L-dopa substrate and 100 μL of sample or positive control solution were mixed and preincubated for 5 min at 37.5 °C, then 50 μL of 100 U/mL tyrosinase was added. Absorbance at 475 nm was measured after 5 min.

Inhibition of mushroom tyrosinase activity was determined as follows:

$$\% \text{ Tyrosinase activity inhibition} = \left[1 - \frac{A1 - A2}{A3 - A4} \right] \times 100$$

where A_1 is the absorbance of substrate, sample and tyrosinase, A_2 is the absorbance of substrate and sample, A_3 is the absorbance of substrate and tyrosinase, and A_4 is the absorbance of substrate. In each case, the median value of triplicate measurements was used.

2.7. Online tyrosinase inhibition profiling

Screening of PLPF extract components for tyrosinase inhibitory capacity was performed using a post-column online biochemical assay (POBA) that was recently developed [33,34] and optimized in our laboratory and previously reported (Fig. 2B). The method is based on the post-column reaction of components with substrate and tyrosinase, and is monitored in real time. Separation was achieved on an HPLC-PDA system (Waters, Milford, MA, USA) using a Kromasil 100-5-C18 column (4.6 mm × 250 mm, 5 μm; AkzoNobel, Sweden) and a binary solvent gradient (A, 0.002% acetic acid in water; B, 100% acetonitrile) at 0.15 mL/min as follows: 0–10 min, 10–20% B; 10–50 min, 20% B; 50–55 min, 20–25% B; 55–100 min, 25% B; 100–115 min, 25–80% B; and 115–120 min, 80% B. Injection volume was 10 μL. Tyrosinase inhibition by individual compounds was evaluated by post-column reaction firstly with substrate
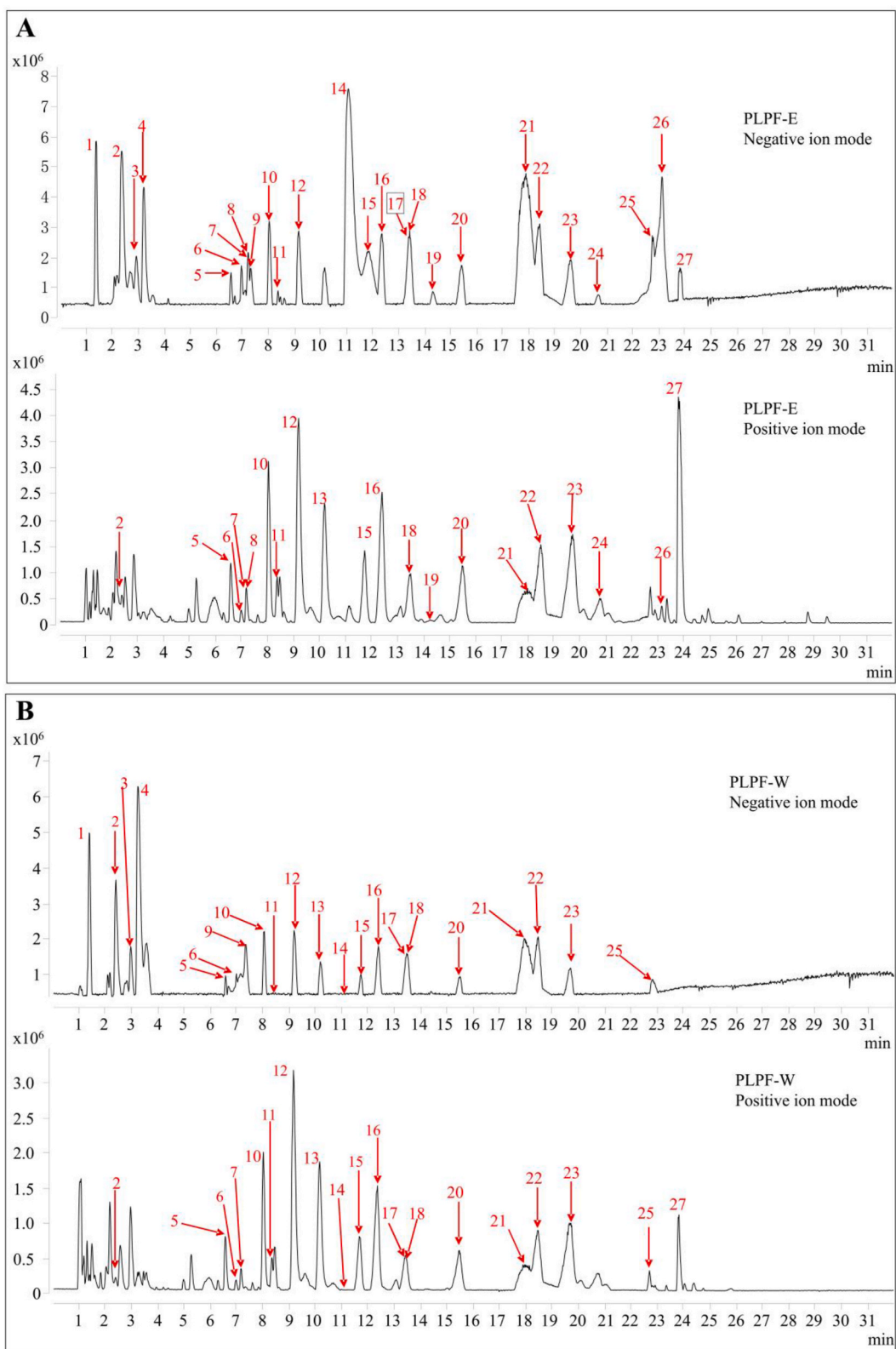
Fig. 3. UPLC-ESI-MS/MS total ion chromatograms of PLPF-E ethanol extract (A) and PLPF-W aqueous extract (B).

Table 1
UPLC-QTOF identification data of compounds detected in PLPF extracts.

No.	Time (min)	Ion	*m/z*	ppm	Mol.	Mol. wt.	Name	MS/MS data
1	1.38	[M − H]⁻	191.0564	4.2	$C_7H_{12}O_6$	192.06	Quinic acid	127.0399; 109.0295; 93.0343; 85.0289; 59.0135
2	2.37	[M − H]⁻	331.0691	7.8	$C_{13}H_{16}O_{10}$	332.07	1-*O*-Galloylglucose	211.0231; 169.0140; 125.0242; 107.0139
3	2.93	[M − H]⁻	331.0676	3.3	$C_{13}H_{16}O_{10}$	332.07	6-*O*-Galloylglucose	211.0215; 169.0136; 125.0242; 107.0139
4	3.21	[M − H]⁻	169.0151	8.3	$C_7H_6O_5$	170.02	Gallic acid	125.0220; 124.0158; 95.0131; 79.0186; 67.0184
5	6.56	[M − H]⁻	495.1513	2.1	$C_{23}H_{28}O_{12}$	496.16	Oxypaeoniflorin	495.1494; 165.0559,137.0252,113.0235; 93.0344
6	6.97	[M − H]⁻	495.1533	6.2	$C_{23}H_{28}O_{12}$	496.16	*ortho*-Oxypaeoniflorin	165.0559; 137.0252; 113.0246; 93.0350
7	7.17	[M − H]⁻	625.1412	1.2	$C_{27}H_{30}O_{17}$	626.15	Quercetin-3,7-diglucoside	625.1321; 463.0846; 301.0342; 299.0289
8	7.22	[M − H]⁻	183.0302	4.7	$C_8H_8O_5$	184.04	Methyl gallate	124.0153; 95.0127; 78.0104; 65.0024
9	7.32	[M − H]⁻	321.0253	2.0	$C_{14}H_{10}O_9$	322.03	Digallic acid	321.0232,169.0138; 125.0243; 79.0183
10	8.03	[M − H]⁻	609.1472	2.7	$C_{27}H_{30}O_{16}$	610.15	Kaempferol-3,7-diglucoside	609.1455; 446.0854; 447.0917; 285.0253; 283.0253
11	8.36	[M − H]⁻	639.1567	0.9	$C_{28}H_{32}O_{17}$	640.16	Isorhamnetin-3,7-diglucoside	639.1537; 477.1017; 315.0504; 313.0351
12	9.19	[M+H]⁺	481.1719	1.9	$C_{23}H_{28}O_{11}$	480.16	Albiflorin	179.0699; 161.0592; 133.0587; 105.0277; 77.0328
13	10.2	[M + NH4]⁺	498.1979	0.7	$C_{23}H_{28}O_{11}$	480.16	Paeoniflorin	179.0698; 161.0622; 151.0746; 133.0644; 105.0693
14	11.08	[M − H]⁻	197.0461	5.6	$C_9H_{10}O_5$	198.05	Ethyl gallate	124.0164; 95.0133; 78.0108; 51.0233
15	11.68	[M − H]⁻	639.1572	1.7	$C_{28}H_{32}O_{17}$	640.16	Astragaloside	639.1545; 477.0095; 314.0427; 299.0193
16	12.37	[M − H]⁻	669.1632	−5.2	$C_{29}H_{34}O_{18}$	670.17	6,3′-Dimethoxyquercetin-diglucoside	669.1642; 344.0535; 329.0301; 301.0343
17	13.33	[M − H]⁻	787.0992	−0.2	$C_{34}H_{28}O_{22}$	788.11	1,2,3,6-Tetra-*O*-galloy-*β*-D-glucopyranose	787.0978; 617.0769; 465.0638; 423.0571
18	13.43	[M − H]⁻	615.1001	2.4	$C_{28}H_{24}O_{16}$	616.11	Quercetin3-*O*-D-(6″-*O*-galloyl)-glucopyranoside	615.0970; 463.0874; 301.0344; 300.0275; 169.0137
19	14.32	[M − H]⁻	300.9992	2.5	$C_{14}H_6O_8$	302.01	Ellagic Acid	300.9997; 283.9951; 200.0110; 173.0241; 145.0294
20	15.43	[M − H]⁻	463.0877	0.1	$C_{21}H_{20}O_{12}$	464.10	Isoquercitrin	301.0325; 300.0273; 271.0246; 255.0294; 151.0033
21	17.89	[M − H]⁻	939.1126	2.4	$C_{41}H_{32}O_{26}$	940.12	1,2,3,4,6-Pentagalloyl glucose	939.1056; 787.1094; 769.0957; 617.0594; 447.0561; 295. 0452; 169.0142
22	18.43	[M − H]⁻	599.1058	3.5	$C_{28}H_{24}O_{15}$	600.11	Kaempferol-3-*O*-(6″-galloyl)-*β*-D-glucopyranosid	599.1037; 447.0831; 313.0561; 285.0432; 271.0444
23	19.6	[M − H]⁻	629.1101	−6.6	$C_{29}H_{26}O_{16}$	630.12	Isorhamnetin-3-*O*-glucoside-6″-gallate	629.1125; 477.1017; 315.0503; 313.0557; 300.0557
24	20.68	[M − H]⁻	477.1043	2.1	$C_{22}H_{22}O_{12}$	478.11	Isorhamnetin-3-*O*-glucoside	477.0971; 314.0423; 299.0187; 285.0395; 271.0240
25	22.77	[M − H]⁻	1091.1224	1.0	$C_{48}H_{36}O_{30}$	1092.13	Hexagalloyl glucose	939.1092; 769.0877; 617.0711; 447.0584; 295.0446
26	23.13	[M − H]⁻	349.0572	3.6	$C_{16}H_{14}O_9$	350.06	Ethyl-P-digallate	197.0452; 169.0139; 140.0107; 124.0166
27	23.78	[M+H]⁺	584.2779	0.	$C_{34}H_{37}N_3O_6$	583.27	N, N′, N″-tris-(*p*-coumaroyl) spermidine	584.2754; 438.2386; 292.2024; 204.1024; 147.0443

reagent (0.5 mM L-dopa) supplied by a second isocratic HPLC pump (Waters, Milford, MA, USA) at 0.4 mL/min, and secondly with 200 U/mL tyrosinase solution (kept on ice during the reaction) supplied by a third isocratic pump at a flow rate of 0.2 mL/min. Parameters including substrate and tyrosinase concentrations and flow rates were previously optimized to maximize sensitivity. The sample-substrate-tyrosinase mixture was passed through a 15 m reaction coil (inner diameter 0.5 mm, outer diameter 1.6 mm) and the degree of inhibition was indicated by the negative peak at 495 nm.

2.8. Antiglycation capacity in a BSA-fructose/glucose system

The formation of total fluorescent AGEs in glycated samples was determined from their fluorescence intensity at excitation/emission wavelengths of 350/450 nm using a SpectraMax i3x microplate reader (Molecular Devices, CA, U.S.A) as previously described [35,36]. Glycated protein was prepared *in vitro* by incubation of BSA with D-glucose (GLC) and D-fructose (FRC). The PLP extract and standards were dissolved in DMSO/water (1:4). BSA (100 μL, 4 mg/mL) was mixed with 50 μL GLC (0.5 M) and 50 μL FRC

(0.5 M) in 20 mM sodium phosphate buffer (pH 7.4), then 100 μL of sample was added in a 96-well plate and incubated at 37.5 °C for 7 days. All solutions were stored under aseptic conditions and passed through 0.22 μm syringe filters before use. Assays were performed in triplicate, and rutin was used as a positive control. Inhibition of the formation of fluorescent AGEs was calculated as follows:

$$\text{Inhibition } (\%) = 1 - \left[\left(IF_{sample} - IF_{sample_{control}} \right) \Big/ \left(IF_{control} - IF_{blank_{control}} \right) \right] \times 100.$$

where IF_{sample} is fluorescence intensity in the presence of samples and BSA, $IF_{sample\ control}$ is intensity in the presence of samples without BSA, $IF_{control}$ is intensity without samples, and $IF_{blank\ control}$ is intensity without samples and BSA. Various sample concentrations were used to determine the half maximal inhibitory concentration (IC_{50}).

2.9. Anticyclooxygenase-2 assay

The capacity to inhibit COX-2 partially reflects anti-inflammatory properties and was determined according to a COX-2 Inhibitor Screening Kit protocol (No.S0168, Beyotime). Celcoxib (a COX-2-inhibiting drug) was used as a positive control. Results are expressed as IC_{50} (in μg/mL or μM), indicating the sample concentration at which enzyme activity is reduced by 50%.

2.10. Collagenase inhibition assay

Collagenase inhibition activity was determined using a previously reported method with some modifications [37]. Collagenase from *Clostridium histolyticum* (ChC) was added to Tricine buffer (50 mM, pH 7.5, 400 mM NaCl, and 10 mM CaCl$_2$) at a concentration of 1 unit/mL. The substrate FALGPA (1 mM) was also dissolved in Tricine buffer. ChC inhibition was determined as follows: 50 μL of sample was incubated with 50 μL of ChC solution for 10 min at 37.5 °C, then 100 μL of FALGPA solution was added to initiate the reaction. The absorbance at 335 nm was measured at 5 min intervals for 30 min using a Beckmann Dual Spectrometer (Beckman, Fullerton, CA, USA). Sample solvent was used as a negative control and EGCG as a positive control. Triplicate measurements were made and IC_{50} values determined from dose-response curves.

$$chc\ inhibion(\%) = \frac{\Delta OD_{control} - \Delta OD_{SamPle}}{\Delta OD control} \times 100$$

where $\Delta OD_{control}$ is the absorbance difference after 30 min for the buffer, collagenase, sample solvent, and substrate system, and ΔOD_{sample} is the absorbance difference for buffer, collagenase, samples, and substrate.

2.11. Statistical analyses

Data were processed using GraphPad software, with results expressed as mean ± standard deviation (SD). Significance was evaluated by one-way ANOVA and Tukey's test: $p \geq 0.05$ (not significant), *$p < 0.05$, **$p < 0.01$, ***$p < 0.001$, and ****$p < 0.0001$. Matrix-bubble and radar diagram analyses of compounds and activities were carried out using the official Hiplot website.

3. Results and discussion

3.1. Identification of compounds by UPLC-QTOF-MS/MS

After optimizing the separation of compounds in the PLPF extracts, 27 compounds were tentatively identified based on retention time, elution sequence, ultraviolet–visible absorption spectra characteristics, mass spectrometric fragmentation, and comparison with reference standards. These included four monoterpene glycosides (compounds **5–6** and **12–13**), six phenols (**1**, **4**, **8–9**, **14**, and **26**), six tannins (**2–3**, **17**, **19**, **21**, and **25**), ten flavonoids (**7**, **10–11**, **15–16**, **18**, **20**, and **22–24**), and a hydroxycinnamic acid amide (**27**). Total ion chromatograms of PLPF-E and PLPF-W are shown as Fig. 3A and B, respectively, and detailed identification information is listed in Table 1. The retention times and fragmentation patterns of compounds **1**, **4**, **5**, **8**, **10–15**, **17**, **19–21**, and **24** were compared with reference standards.

The MS data and retention times of compounds **1**, **4**, and **19** closely matched quinic acid, gallic acid, and ellagic acid standards, respectively. The highest UV absorption peak of compounds **8**, **9**, **14** and **26** was consistent with compound **4**, indicating these were gallic acid derivatives. The [M − H]⁻ molecular ions of compounds **8** at m/z 183 and **14** at m/z 197 indicated they were methyl and ethyl gallate, respectively. Compound **9** exhibited a [M − H]⁻ ion at m/z 321 and MS/MS fragments at m/z 169 (gallic acid, $C_7H_5O_5$) and m/z 125 ($C_6H_5O_5$) due to the loss of [M-H-152]⁻ and [M-H-CO$_2$]⁻, so was tentatively identified as digallic acid [38]. Compound **26** exhibited a [M − H]⁻ molecular ion at m/z 349 and a fragment at m/z 197 [M-H-152]⁻, indicating the presence of an ethyl gallate group and identifying it as ethyl-P-digallate.

Gallotannins, which contain glucose and gallic acid moieties, were relatively abundant in the PLPFs [39]. Tannins tend to from a series of MS/MS product ions resulting from the successive loss of gallic acid (170 Da) and a galloyl group (152 Da). Compounds **2** and **3** exhibited the same [M − H]⁻ molecular ion at m/z 331 and fragment at m/z 169, suggesting gallic acid following the loss of hexose. These compounds were tentatively identified as 1-O-galloylglucose and 6-O-galloylglucose, respectively [40–42]. The [M − H]⁻ molecular ion for compound **17** at m/z 787 matched tetragalloylglucose. Fragments of [M-gallic acid]⁻ at m/z 617 and [M-gallic acid-152]⁻ at m/z 465 were also observed. Similarly, **21** exhibited a [M − H]⁻ ion at m/z 939, suggesting it was pentagalloylglucose, while the
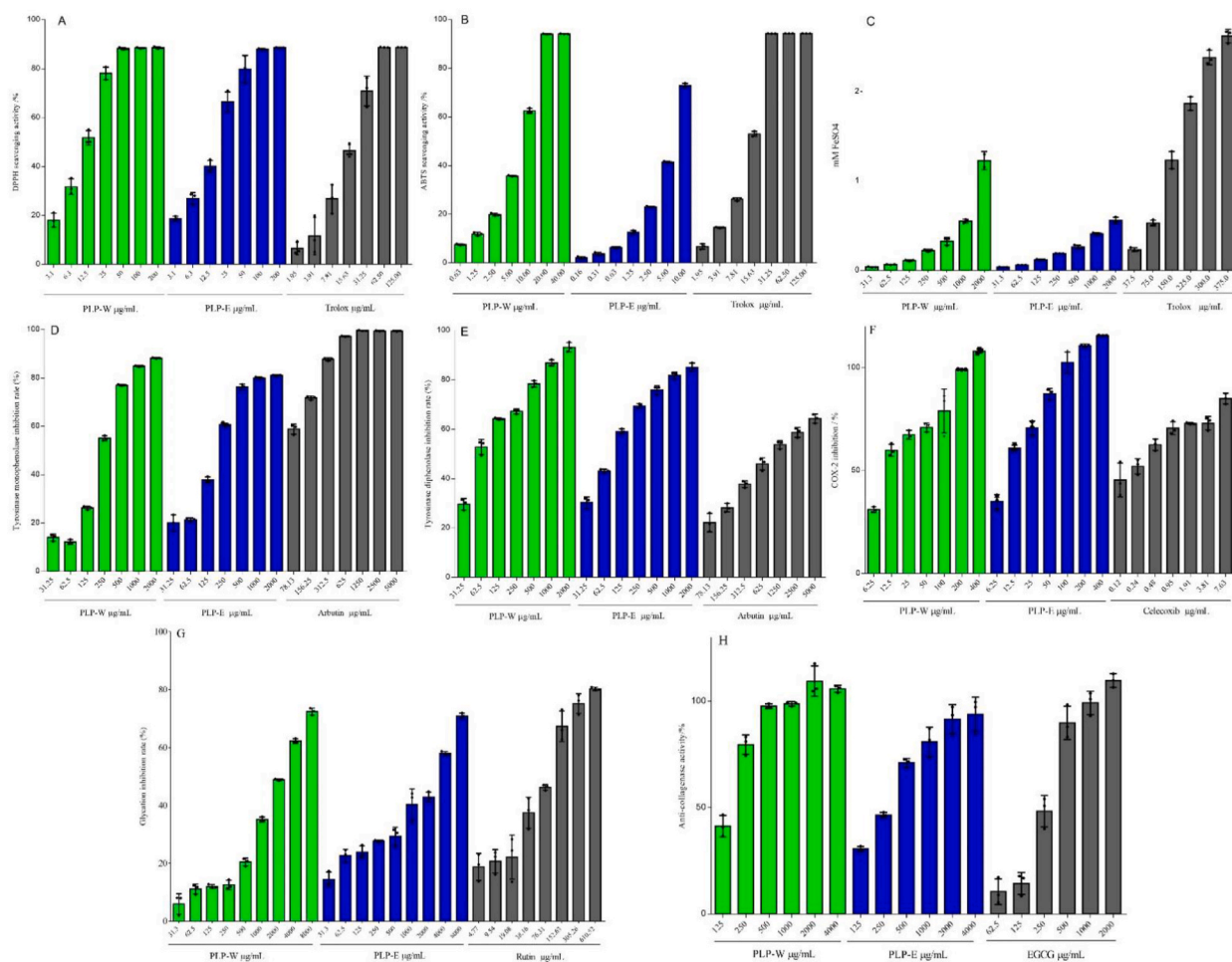
Fig. 4. Skin-related bioactivities of PLPF extracts: DPPH scavenging (A), ABTS scavenging (B), FRAP value (C), monophenolase (tyrosinase) inhibition (D), diphenolase (tyrosinase) inhibition (E), COX-2 inhibition (F), antiglycation activity (G), and anticollagenase activity (H).

fragments at m/z 787, 769, 617, 447 and 295 were attributed to single or consecutive losses of galloyl and/or gallic acid. Comparison with standard retention times indicated that **17** and **21** were 1,2,3,6-tetra-*O*-galloy-*β*-D-glucopyranose and 1,2,3,4,6-pentagalloyl glucose, respectively. Compound **25** exhibited a parent ion at m/z 1091 and a daughter ion at m/z 939 (attributed to loss of a galloyl unit) that generated further fragments at m/z 769, 617, 447, and 295, suggesting it was hexagalloylglucose [43].

Monoterpene glycosides were another class of bioactive compounds extracted from the PLPFs [44]. Compounds **12** and **13** were identified as albiflorin and paeoniflorin, respectively, by comparing their MS/MS fragments with reference standards [45]. Compounds **5** and **6** produced the same negative mode molecular ion at m/z 495 and similar fragments at m/z 165, 137, 113, and 93, identifying them as oxypaeoniflorin and *ortho*-oxypaeoniflorin, respectively.

PLPFs are also a rich source of flavonoids. Compounds **10**, **11**, **15**, **20**, and **24** were identified as kaempferol-3,7-diglucoside, isorhamnetin-3,7-diglucoside, astragaloside, isoquercitrin, and isorhamnetin-3-*O*-glucoside, respectively, by comparing their fragment ions with online reference standards. Compound **7** produced fragments at m/z 625, 463, and 301, suggesting it was quercetin-3,7-diglucoside [46,47]. Compound **16** exhibited an [M − H]⁻ ion at m/z 669 and daughter ions at m/z 344 and 301, and was likely to be 6,3′-dimethoxyquercetin-di-*O*-glucoside [48]. A mass loss of 314 indicates the presence of a galloylhexoside moiety, and this was observed with compounds **18**, **22**, and **23**. For example, the spectrum of **18** contained a fragment at m/z 463 resulting from the loss of 152 (a galloyl moiety) from its [M − H]⁻ molecular ion at m/z 615 [49]. A further loss of 162 confirmed the presence of a hexoside moiety [50,51], so **18** was tentatively identified as quercetin-3-*O*-D-(6″-*O*-galloyl)-glucopyranoside. Similarly, **22** and **23** were tentatively identified as kaempferol-3-*O*-(6″-galloyl)-glucopyranosid [52,53] and isorhamnetin-3-*O*-glucoside-6″-gallate, respectively.

Polyamines are ubiquitous in the plant kingdom, particularly in flowers and seeds [54]. Compound **27** exhibited a [M+H]⁺ at m/z 584 and fragments at m/z 438 and 292 following neutral losses of one or two coumaroyl moieties (m/z 146). Further cleavage of amide bonds produced characteristic coumaroyl ions (m/z 147) originating from neutral losses of spermidine (m/z 145). Although a reference standard was lacking, **27** was identified as N,N′,N″-tris-(*p*-coumaroyl) spermidine based on literature sources [55,56].

Table 2
Various bioactivities of the PLPF extracts.

|	Sample	Antioxidant			Anti-tyrosinase		Antiglycation	Anti-collagenase	Anti-COX-2
		DPPH	ABTS	FRAP	TYR	DOPA	BSA	COL	COX-2
		IC$_{50}$ (μg/mL)		EC1 (μg/mL)	IC$_{50}$ (μg/mL)				
Extract	PLPF-W	11.12 ± 1.15	6.53 ± 0.12	383.04 ± 15.57	232.90 ± 4.40	72.14 ± 4.82	2155.00 ± 212.94	144.50 ± 12.76	11.95 ± 0.97
	PLPF-E	15.42 ± 1.91	5.67 ± 0.06	647.41 ± 40.42	189.77 ± 10.21	89.21 ± 4.21	2252.33 ± 83.86	262.63 ± 15.71	10.06 ± 0.82
Positive control	Trolox	16.60 ± 1.55	12.93 ± 0.03	129.73 ± 3.29					
	Arbutin				62.22 ± 4.22	1083.63 ± 188.61			
	Rutin						74.56 ± 6.38		
	EGCG							247.43 ± 19.81	
	Celecoxib								0.17 ± 0.06
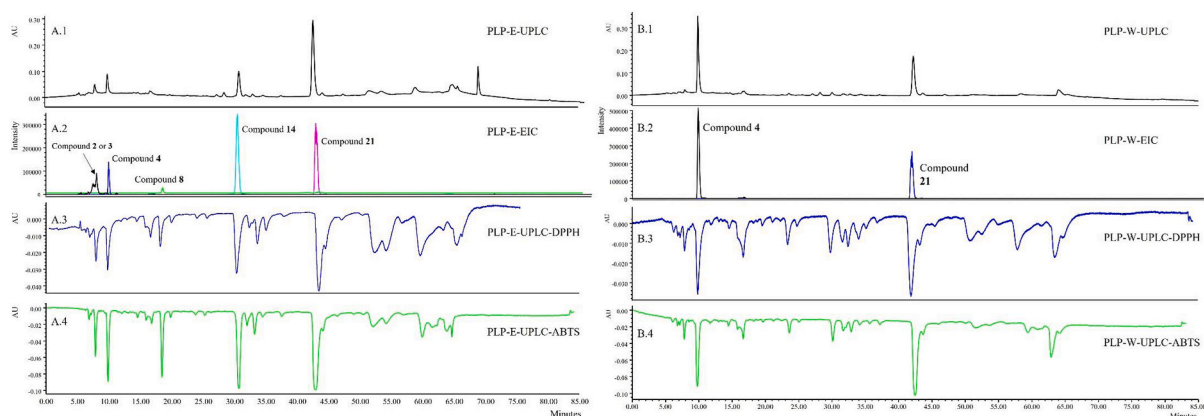
Fig. 5. Antioxidant capacities of PLPF-E and PLPF-W extracts: 280 nm chromatograms (A.1, B.1), extracted ion chromatogram (A.2, B.2), UPLC-UV-DPPH• scavenging profiles with negative peak at 517 nm (A.3, B.3), and UPLC-UV-ABTS•+ scavenging profiles with negative peak at 739 nm (A.4, B.4). Compounds **2** (or **3**), **4**, **8**, **14**, and **21** were identified as galloylglucose, gallic acid, methyl gallate, ethyl gallate, and 1,2,3,4,6-pentagalloyl glucose, respectively.

3.2. Antioxidant capacity by DPPH, ABTS, FRAP, and online HPLC-DPPH/ABTS assays

A portfolio of antioxidant assays is vital for a comprehensive evaluation of natural products, so DPPH, ABTS, and FRAP assays were used to assess the antioxidant potential of the extracts and their major compounds. Both PLPF-W and PLPF-E exhibited concentration-dependent antioxidant activity in the range 3.1–200 μg/mL (Fig. 4A, B, 4C, and Table 2). The IC$_{50}$ for scavenging DPPH radicals was 11.12 ± 1.15 μg/mL (PLPF-W) and 15.42 ± 1.91 μg/mL (PLPF-E), in contrast to 16.60 ± 1.55 μg/mL for Trolox. In the ABTS assay, the IC$_{50}$ was 6.53 ± 0.12 μg/mL for PLPF-W and 5.67 ± 0.06 μg/mL for PLPF-E, which were substantially lower than for Trolox (12.93 ± 0.03 μg/mL). In the FRAP assay, the EC$_1$ values were 383.0 ± 15.6 μg/mL for PLPF-W and 647.4 ± 40.4 μg/mL for PLPF-E, while Trolox was 129.7 ± 3.3 μg/mL. Thus, the PLPF extracts exhibited outstanding antioxidant properties, which is consistent with previous studies [44].Sensitive online UPLC-DPPH and UPLC-ABTS assays were performed simultaneously to rapidly screen for the major phytochemicals responsible for the antioxidant activity of the PLPF extracts (Fig. 5). The upper positive chromatogram shows the profiles of PLPF extracts at 280 nm (A.1, B.1), and extracted ion chromatograms of PLPF extracts are shown as A.2 and B.2, while the lower negative chromatograms show the compound responses after reaction with DPPH radical at 517 nm (A.3, B.3) and ABTS radical at 729 nm (A.4, B.4). Given that the size of a negative peak is proportional to the compound's antioxidant effect, five compounds in the PLPF-E extract (**2** [or **3**], **4**, **8**, **14**, and **21**) and two in the PLPF-W extract (**4** and **21**) dominated the scavenging of both DPPH• and ABTS•+. Compounds **2** (or **3**), **4**, **8**, **14** and **21** were identified as galloylglucose, gallic acid, methyl gallate, ethyl gallate and 1,2,3,4,6-pentagalloyl glucose, respectively.

To confirm these findings, specific compounds were selected for more detailed analysis of their antioxidant capacities using offline DPPH, ABTS, and FRAP assays (Table 3). Compounds **4**, **8**, **10**–**11**, **14**–**15**, **17**, **19**–**21**, and **24** exhibited greater scavenging capacities

Table 3
Concentration of gallic acid derivatives in PLPF extracts and the functional activities of selected compounds.

No.	Individual Compounds	Co. of PLPF-W (%)	Co. of PLPF-E (%)	Antioxidant			Anti-tyrosinase		Antiglycation	Anti-collagenase	Anti-COX-2
				DPPH	ABTS	FRAP	TYR	DOPA	BSA	COL	COX-2
				IC50 (μM)		EC1 (μM)	IC50 (μM)				
1	Quinic acid			nd	nd	nd	nd	nd	nd	nd	nd
4	Gallic acid	9.31 ± 0.02	1.96 ± 0.02	36.69 ± 6.67	8.19 ± 0.08	107.51 ± 18.11	nd	1605.00 ± 503.26	72.52 ± 12.31	nd	417.30 ± 119.94
5	Oxypaeoniflorin			nd	322.73 ± 3.29	nd	nd	nd	nd	nd	nd
8	Methyl gallate	0.28 ± 0.02	1.58 ± 0.02	34.95 ± 3.22	14.20 ± 0.10	301.99 ± 39.12	2287.33 ± 38.73	811.77 ± 62.53	nd	nd	17.92 ± 0.66
10	Kaempferol-3,7-diglucoside			nd	30.60 ± 0.51	nd	nd	nd	395.30 ± 30.58	nd	nd
11	Isorhamnetin-3,7-diglucoside			nd	41.68 ± 0.14	2324.30 ± 290.63	nd	nd	4948.33 ± 394.58	nd	378.23 ± 86.22
12	Albiflorin			nd	nd	nd	nd	nd	nd	nd	nd
13	Paeoniflorin			nd	nd	nd	nd	nd	nd	nd	nd
14	Ethyl gallate	nd	2.76 ± 0.05	43.40 ± 5.52	17.74 ± 0.28	145.98 ± 3.20	2565.00 ± 382.46	701.37 ± 48.04	nd	nd	13.42 ± 1.75
15	Astragaloside			>500	21.27 ± 0.05	2459.55 ± 284.98	nd	nd	211.67 ± 59.88	nd	364.77 ± 22.35
17	1,2,3,6-tetra-O-galloy-β-D-glucopyranose	0.41 ± 0.02	0.51 ± 0.05	11.86 ± 0.65	3.59 ± 0.17	129.86 ± 23.18	366.90 ± 21.04	246.73 ± 15.65	2359.67 ± 186.11	272.87 ± 46.13	3.92 ± 0.15
19	Ellagic Acid			67.81 ± 7.35	5.76 ± 0.21	50.33 ± 1.69	nd	nd	>5000	nd	4.62 ± 0.21
20	Isoquercitrin			90.48 ± 12.42	6.51 ± 0.15	334.87 ± 65.29	nd	nd	122.27 ± 19.15	nd	3.42 ± 0.78
21	1,2,3,4,6-pentagalloyl glucose	7.96 ± 0.34	14.93 ± 0.18	8.91 ± 1.24	3.76 ± 0.08	248.33 ± 42.35	175.23 ± 5.99	289.23 ± 16.25	1656.67 ± 359.01	213.40 ± 85.76	4.09 ± 0.43
24	Isorhamnetin-3-O-glucoside			>500	15.26 ± 0.37	2681.88 ± 140.91	nd	nd	78.05 ± 20.59	nd	285.70 ± 14.13
Positive	Trolox			66.39 ± 6.18	51.72 ± 0.13	518.93 ± 13.14					
	Arbutin						228.55 ± 15.51	3980.27 ± 692.80			
	Rutin								122.13 ± 10.46		
	EGCG									539.81 ± 43.21	
	Celecoxib										0.44 ± 0.15

nd: not detected.
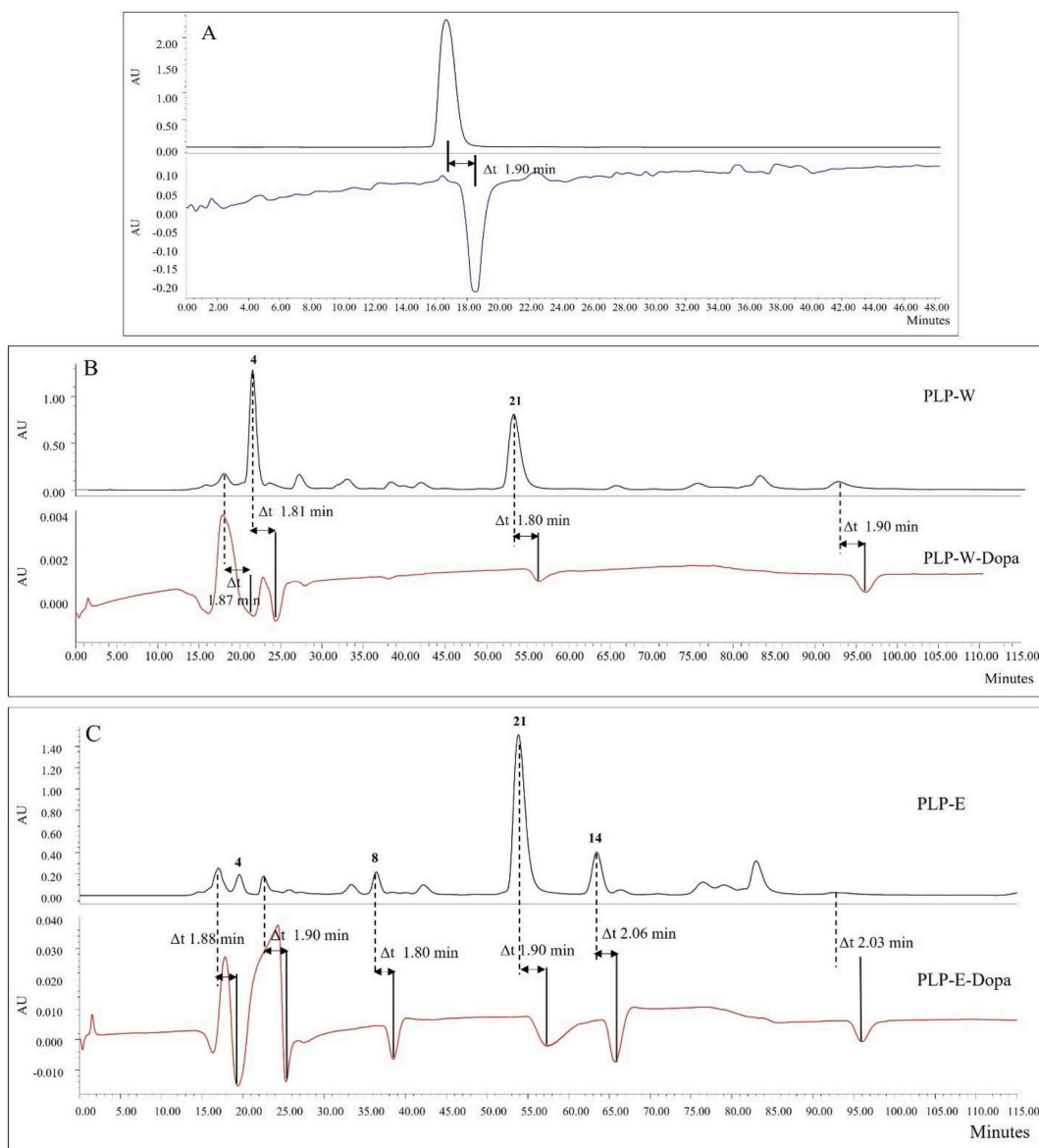Co.: concentration.

Fig. 6. POBA UV chromatograms of (A) Vc, (B) PLPF-W extract, and (C) PLPF-E extract.

for ABTS radical than the Trolox positive control, with IC$_{50}$ values from 3.59 ± 0.17 μM (**17**) to 41.68 ± 0.14 μM (**11**). However, only compounds **4**, **8**, **14**, **17**, and **19**–**21** showed notable scavenging of DPPH, with IC$_{50}$ from 8.91 ± 1.24 μM (**21**) to 90.48 ± 12.42 μM (**20**), and FRAP, with EC$_1$ from 50.33 ± 1.69 μM (**19**) to 334.87 ± 65.29 μM (**20**). The combination of online screening and offline antioxidant assays demonstrates that gallic acid derivatives are the primary contributors to the antioxidant capacity of PLPF extracts.

3.3. Online screening for tyrosinase inhibition

Tyrosinase catalysis comprises two steps: firstly, the generation of dopa from tyrosine substrate by the hydroxylation of mono-phenol to diphenol; and secondly, the oxidation of dopa to dopaquinone by the oxidation of the diphenol to quinone [32]. The tyrosinase-inhibiting capacity of the PLPF extracts was evaluated via both monophenolase and diphenolase assays using arbutin (which is widely used as an active cosmetic) as a positive control (Fig. 4D and Table 2) [57]. PLPF-E and PLPF-W demonstrated notable monophenolase-inhibiting capacities (IC$_{50}$ 189.8 ± 10.2 μg/mL and 232.9 ± 4.4 μg/mL, respectively) that were similar to arbutin (IC$_{50}$ 228.6 ± 15.5 μg/mL). By contrast, PLPF-E and PLPF-W exhibited much stronger diphenolase-inhibiting activities (IC$_{50}$ 72.1 ± 4.8 μg/mL and 89.2 ± 4.2 μg/mL, respectively) than arbutin (IC$_{50}$ 3980 ± 693 μg/mL).

POBAs are an effective way of identifying the principal active components in plant extracts, as they help to avoid false positives and improve screening accuracy [58,59]. The PLPF extract components were separated by HPLC and eluted sequentially to mix with a

substrate solution in the first reaction coil, then pumped continuously into an enzyme solution in the second coil. The inhibition profile of the eluted compounds is visualized as negative peaks. While the application of POBA to TYR has previously been reported in detail [33,34], some key factors still needed to be optimized. To ensure sufficient time for the enzymatic catalysis, L-dopa was chosen as the substrate because it is catabolyzed more quickly than tyrosine. To optimize both the separation of the extract components and the degree of catalysis, the overall flow rate of the assay system was set at 0.75 mL/min, with the HPLC column flow rate being 0.15 mL/min. An organic modifier such as acetonitrile and a volatile acid such as acetic acid, are necessary in the mobile phases for effective separation of PLPF compounds. However, both can lower TYR activity, or even denature it. This inhibition should be limited to less than 50% [60]. Thus, the aqueous mobile phase was limited to 0.002% acetic acid and a maximum of 25% acetonitrile was introduced during compound elution, as TYR activity was reduced by 57.4% by the terminal mobile phase. Finally, ascorbic acid (Vc), a potent TYR inhibitor was used to validate the reliability of the method. The UV chromatogram in Fig. 6A shows that Vc was detected at 16.67 min, while its effect on TYR was observed at 18.57 min, demonstrating a delay of 1.9 ± 0.1 min (n = 3).

The HPLC and bioactivity profiles of the extracts are shown in Fig. 6B and C. Peaks **4** and **21** of PLPF-W and peaks **8**, **14** and **21** of PLPF-E show negative responses, demonstrating their diphenolase-inhibiting properties. Compounds **4**, **8**, **14** and **21** were tentatively identified as gallic acid, methyl gallate, ethyl gallate and 1,2,3,4,6-tetra-O-galloy-β-glucose, respectively. Lack of reference standards prevented the identification of the other compounds with negative peaks (the last peak, in particular, demonstrated a strong inhibitory effect).

The effects of selected PLPF extract compounds on TYR were investigated (Table 3). Surprisingly, only compounds **17** (IC$_{50}$ 366.9 $\pm$ 21.0 μM) and **21** (IC$_{50}$ 175.2 $\pm$ 6.0 μM) demonstrated significant monophenolase inhibition, with the latter displaying the strongest effect [22]. Monophenolase inhibition by the gallic acid derivatives followed the trend: galloylglucose > gallate esters > gallic acid. By contrast, compounds **4**, **8**, **14**, **17**, and **21** (gallic acid and its derivatives) exhibited excellent or moderate diphenolase inhibition, in accordance with previous reports [31]. Diphenolase inhibition followed the same trend as monophenolase inhibition: galloylglucose > gallate esters > gallic acid. This suggests that TYR inhibition is positively correlated with molecular weight, as previously demonstrated with various tannins [61]. It is likely that the active compounds described above act synergistically to inhibit TYR. The concentrations of gallic acid and its derivatives were also measured in PLPF-W and PLPF-E (Table 3). Compounds **4** and **21** dominated PLPF-W, being present at $9.31 \pm 0.02\%$ and $7.96 \pm 0.34\%$, respectively, which corresponds with the bioactivity profile of this extract. Compounds **4**, **8**, **14**, and **21** were present in PLPF-E at $1.96 \pm 0.02\%$, $1.58 \pm 0.02\%$, $2.76 \pm 0.05\%$, and $14.93 \pm 0.18\%$, respectively. Compound **4** exhibited relatively weak inhibition of TYR despite its significant concentration. Consequently, **8**, **14**, and **21** are considered to be the principal active components, in accordance with the bioactivity profile of PLPF-E.

3.4. COX-2 inhibition by PLPF extracts and principal compounds

COX-2 is an inducible enzyme that produces prostaglandins but also generates ROS. Consequently, it is regarded as a pathological enzyme that is a major contributor to inflammation [62]. COX-2 inhibitors can cause a dramatic drop in the concentration of ROS and are often promising antioxidant compounds [63]. COX-2 inhibition was used to evaluate the anti-inflammatory effects of PLPF extracts and their principal compounds against celecoxib, a well-known selective COX-2 inhibitor. PLPF extracts showed considerable concentration-dependent COX-2 inhibition in the concentration range 31.3–2000 μg/mL (Fig. 4F and Table 2). IC$_{50}$ was 11.95 ± 0.97 μg/mL for PLPF-W, 10.06 ± 0.82 μg/mL for PLPF-E, and 0.17 ± 0.06 μg/mL for celecoxib, showing that PLPF extracts could be used as COX-2 inhibitors.

To tentatively identify the source of this inhibition, 15 of the principal compounds were studied in an *in vitro* assay system (Table 3). Again, celecoxib was a highly effective inhibitor of COX-2 (IC$_{50}$ 0.44 ± 0.15 μM). Compounds **8**, **14**, **17**, and **19–21** also exhibited inhibitory properties, with IC$_{50}$ from 3.42 ± 0.78 μM (**20**) to 17.92 ± 0.66 μM (**8**), suggesting that the anti-inflammatory properties of PLPF-E and PLPF-W were partly attributable to these compounds. Compounds **4**, **11**, **15**, and **24** displayed weak inhibition (IC$_{50}$ above 200 μM), while **1**, **5**, **10**, and **12–13** showed none. Isoquercitrin (**20**) exhibited greater COX-2 inhibition than the isorhamnetin glycosides (**11**, **15**, and **24**), while kaempferol glycoside (**10**) showed no activity, which agrees with previous reports [64,65] and indicates that flavonoid aglycones are crucial to this property of the PLPF extracts. COX-2 inhibition by gallic acid derivatives showed a similar trend to TYR inhibition: galloylglucose > gallate esters > gallic acid.

3.5. Antiglycation properties of PLPF extracts and principal compounds

Incubation of reducing sugars and BSA induces the production of fluorescent AGEs [66]. PLPF-W and PLPF-E reduced the levels of fluorescent AGEs in a concentration-dependent manner, with IC$_{50}$ of 2155 ± 213 μg/mL and 2236 ± 85 μg/mL, respectively (Fig. 4G and Table 2). Rutin, a known antiglycation compound [67,68], was strongly inhibitory, with an IC$_{50}$ of 74.56 ± 6.38 μg/mL.

Fifteen compounds were also analyzed *in vitro*. Compounds **4**, **10**, **15**, **20**, and **24** strongly inhibited AGE formation (Table 3). Compounds **10**, **15**, **20**, and **24** were identified as flavonoids, namely kaempferol-3,7-diglucoside, astragaloside, isoquercitrin, and isorhamnetin-3-O-glucoside, while **4** was gallic acid (a phenolic acid), consistent with previous reports [9]. Compound **4** (IC$_{50}$ 72.52 ± 12.31 μM) was the most effective of these AGE inhibitors, followed by **24**, **20**, **15**, and **10** (IC$_{50}$ 78.05 ± 20.59, 122.3 ± 19.2, 211.7 ± 59.9, and 395.3 ± 30.6 μM, respectively). However, the gallic acid glycoside derivatives **8**, **14**, **17**, and **21** exhibited weak or no inhibition. Compounds **11**, **17**, and **21** displayed relatively weak activity (IC$_{50}$ above 1000 μM), while **1**, **5**, **8**, and **12–14** exhibited no activity. Although several studies have reported a positive correlation between potency of AGE inhibition and antioxidant activity [8], this study found no such connection, with compounds **8**, **14**, **17**, and **21** having powerful antioxidant properties but weak AGEs inhibition effects. Flavonoids were the primary inhibitors of nonenzymatic glycation.
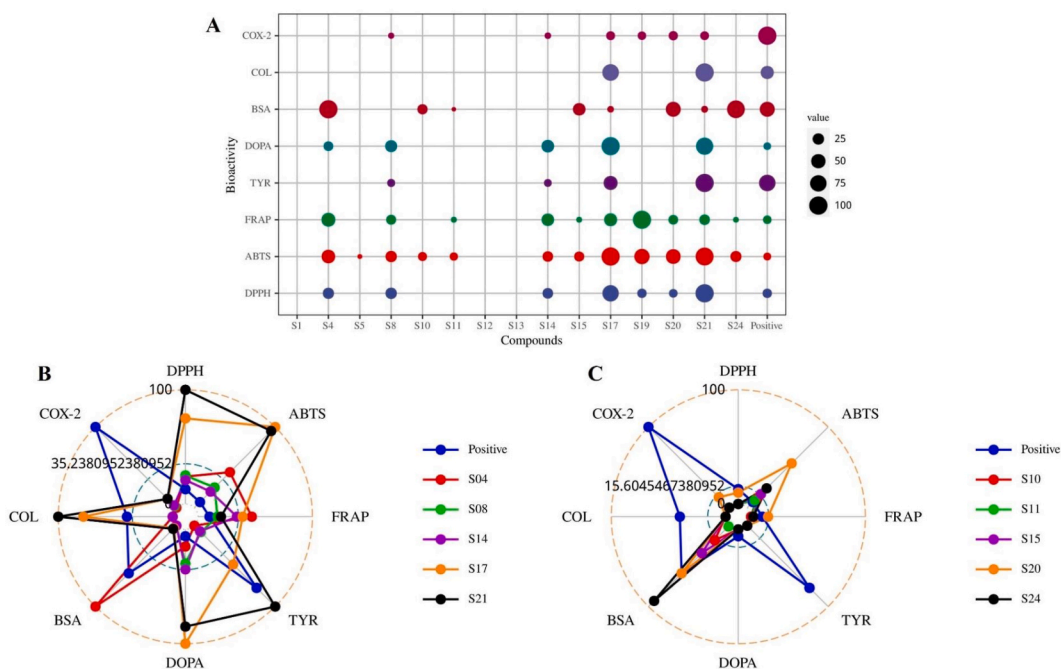
Fig. 7. Matrix-bubble diagram of compound bioactivities (A), and radar diagrams of gallic acid and derivatives (B) and the flavonoids (C).

3.6. Collagenase inhibition by PLPF extracts and principal compounds

Collagen, a major protein in the dermis, is responsible for the skin's tensile strength and is degraded primarily by collagenase, so the importance of finding effective collagenase inhibitors for maintaining the skin's supportive framework is evident. Fig. 4H and Table 2 show that PLPF-E and PLPF-W were potent inhibitors of collagenase, with IC_{50} of 262.6 ± 15.7 and 144.5 ± 12.8 μg/mL, respectively. The positive control EGCG, a frequently used collagenase inhibitor [69], had an IC_{50} of 247.43 ± 19.81 μg/mL, in line with a previous report [37].

It is notable that of all the isolated compounds only **7** and **21** displayed significant anticollagenase properties, with IC_{50} of 272.9 ± 46.1 μM and 213.4 ± 85.8 μM, respectively (Table 3), both being more potent than EGCG (IC_{50} of 539.81 ± 43.21 μM). Given the high concentration of **21** in PLPF [22], it can be speculated that 1,2,3,4,6-pentagalloyl glucose is the main antiglycation component.

3.7. Visualization of compound bioactivities

The bioactivities of the major compounds were visualized using matrix-bubble and radar diagrams. In the matrix-bubble diagram, the larger bubbles indicate stronger bioactivities (Fig. 7A). Compounds **1**, **12**, and **13** made no contribution to any bioactivity. Each color in the radar maps (Fig. 7B and C) represents a bioactivity, with more potent compounds being farther from the center of the circle. Gallic acid and its derivatives are peripheral in their radar map, while the flavonoids are closer to the center, except for antiglycation of BSA. Thus, the main antioxidant, anti-TYR, anticollagenase, and anti-COX2 compounds were gallic acid and its derivatives, while the antiglycation components were mainly flavonoids.

4. Conclusions

Both aqueous and ethanol extracts of PLPF exhibit notable antioxidant and inhibitory effects on TYR, COX-2, collagenase, and protein glycation.Twenty-seven compounds were tentatively identified by UPLC/PDA-QTOF-ESI-MS/MS, including four monoterpene glycosides, six phenols, six tannins, ten flavonoids, and a hydroxycinnamic acid amide. This study is a valuable reference for the development and application of POBA-based online antioxidant and TYR inhibitor screening assays, which can accelerate the drug discovery process. Bioactivity-based screening assays combined with conventional quantitative biochemical assays showed that gallic acid derivatives are the primary contributors to the antioxidant and anti-TYR capacity of PLPF extracts. The major flavonoids tended to be collaborative inhibitors of AGEs, while the gallic acid derivatives may also be responsible for inhibiting collagenase and COX-2. PLPF and its principal compounds are shown to be promising candidates for development as novel pharmaceutical and cosmetic agents.

Author contribution statement

Huiji Zhou: Conceived and designed the experiments; Performed the experiments; Analyzed and interpreted the data; Wrote the paper.

Tingzhao Li, Bo Li, Shuai Sun: Contributed reagents, materials, analysis tools or data.

Data availability statement

Data will be made available on request.

Additional information

No additional information is available for this paper.

Declaration of competing interest

The authors declare that they have no known competing financial interests or personal relationships that could have appeared to influence the work reported in this paper.

References

[1] A. da Costa Gomes, et al., Antioxidant and antiglycation activities and inhibitory action of Passiflora cincinnata on collagenase, elastase and tyrosinase: in vitro and in silico study, Biocatal. Agric. Biotechnol. 44 (2022), 102464.
[2] J.E. Rundhaug, S.M. Fischer, Cyclo-oxygenase-2 plays a critical role in UV-induced skin carcinogenesis, Photochem. Photobiol. 84 (2) (2008) 322–329.
[3] L. Wei, et al., Antioxidant properties, anti-SARS-CoV-2 study, collagenase and elastase inhibition effects, anti-human lung cancer potential of some phenolic compounds, J. Indian Chem. Soc. 99 (4) (2022), 100416.
[4] M. Fournière, et al., Poly-and oligosaccharide ulva sp. Fractions from enzyme-assisted extraction modulate the metabolism of extracellular matrix in human skin fibroblasts: potential in anti-aging dermo-cosmetic applications, Mar. Drugs 19 (3) (2021) 156.
[5] S. Zhang, E. Duan, Fighting against skin aging: the way from bench to bedside, Cell Transplant. 27 (5) (2018) 729–738.
[6] F.S.S. Deniz, I.E. Orhan, H. Duman, Profiling cosmeceutical effects of various herbal extracts through elastase, collagenase, tyrosinase inhibitory and antioxidant assays, Phytochem. Lett. 45 (2021) 171–183.
[7] S. Ullah, et al., Observed changes in temperature extremes over China–Pakistan Economic Corridor during 1980–2016, Int. J. Climatol. 39 (3) (2019) 1457–1475.
[8] I. Guenaou, et al., Bioactive compounds from ephedra fragilis: extraction optimization, chemical characterization, antioxidant and AntiGlycation activities, Molecules 26 (19) (2021) 5998.
[9] L. Spagnuolo, et al., Antioxidant and antiglycation effects of polyphenol compounds extracted from hazelnut skin on advanced glycation end-products (AGEs) formation, Antioxidants 10 (3) (2021) 424.
[10] Z. Alikhani, et al., Advanced glycation end products enhance expression of pro-apoptotic genes and stimulate fibroblast apoptosis through cytoplasmic and mitochondrial pathways, J. Biol. Chem. 280 (13) (2005) 12087–12095.
[11] Y. Ogura, et al., Dermal carbonyl modification is related to the yellowish color change of photo-aged Japanese facial skin, J. Dermatol. Sci. 64 (1) (2011) 45–52.
[12] E.J. Lee, J.Y. Kim, S.H. Oh, Advanced glycation end products (AGEs) promote melanogenesis through receptor for AGEs, Sci. Rep. 6 (1) (2016) 1–11.
[13] H.M. Semchyshyn, Reactive carbonyl species in vivo: generation and dual biological effects, Sci. World J. 2014 (2014).
[14] Y. Yang, et al., Characterization of phytochemicals in the roots of wild herbaceous peonies from China and screening for medicinal resources, Phytochemistry 174 (2020), 112331.
[15] Q. Fu, et al., Paeonidanins F-H: Three new dimeric monoterpene glycosides from Paeonia lactiflora and their anti-inflammatory activity, Phytochem. Lett. 13 (2015) 386–389.
[16] M. Zhao, et al., Anti-inflammatory effects of paeoniflorin from Paeonia lactiflora Pall. on human corneal epithelial cells and a mouse model of dry eye disease, RSC Adv. 9 (23) (2019) 12998–13006.
[17] K.M. Adki, Y.A. Kulkarni, Chemistry, pharmacokinetics, pharmacology and recent novel drug delivery systems of paeonol, Life Sci. 250 (2020), 117544.
[18] X.-j. Zhang, et al., The Analgesic Effect of paeoniflorin on neonatal maternal separation–induced visceral hyperalgesia in rats, J. Pain 9 (6) (2008) 497–505.
[19] L. Liu, et al., Composition and antioxidant activity of Paeonia lactiflora petal flavonoid extract and underlying mechanisms of the protective effect on H2O2-induced oxidative damage in BRL3A cells, Horticultural Plant Journal 9 (2) (2022) 335–344.
[20] X. Wang, et al., Isolation and purification of four flavonoid constituents from the flowers of Paeonia suffruticosa by high-speed counter-current chromatography, J. Chromatogr. A 1075 (1–2) (2005) 127–131.
[21] S.-M. Lee, M.-Y. Yoon, H.-R. Park, Protective effects of Paeonia lactiflora pall on hydrogen peroxide-induced apoptosis in PC12 cells, Biosc. Biotech. Biochem. 72 (5) (2008) 1272–1277.
[22] A.A. Magid, et al., In vitro tyrosinase inhibitory and antioxidant activities of extracts and constituents of paeonia lactiflora pall, Flowers, Nat. Prod. J 7 (3) (2017) 237–245.
[23] L. Weixing, et al., Nutritional evaluation of herbaceous peony (Paeonia lactiflora Pall.) petals, Emir. J. Food Agric. (2017) 518–531.
[24] M.-C. Liu, et al., A simple and convenient method for the preparation of antioxidant peptides from walnut (Juglans regia L.) protein hydrolysates, Chem. Cent. J. 10 (1) (2016) 1–11.
[25] R. Re, et al., Antioxidant activity applying an improved ABTS radical cation decolorization assay, Free Radical Biol. Med. 26 (9–10) (1999) 1231–1237.
[26] I.F. Benzie, J.J. Strain, The ferric reducing ability of plasma (FRAP) as a measure of "antioxidant power": the FRAP assay, Anal. Biochem. 239 (1) (1996) 70–76.
[27] A. Wojdyło, P. Nowicka, Profile of phenolic compounds of Prunus armeniaca L. leaf extract determined by LC-ESI-QTOF-MS/MS and their antioxidant, anti-diabetic, anti-cholinesterase, and anti-inflammatory potency, Antioxidants 10 (12) (2021) 1869.
[28] N. Nantarat, et al., Sesaminol diglucoside isolated from black sesame seed cake and its antioxidant, anti-collagenase and anti-hyaluronidase activities, Food Biosci. 36 (2020), 100628.
[29] W. Wang, et al., On-line HPLC-DPPH bioactivity-guided assay for isolated of antioxidative phenylpropanoids from Qinghai-Tibet Plateau medicinal plant Lancea tibetica, J. Chromatogr. B 1106 (2019) 1–10.
[30] I.P. Turkiewicz, et al., ABTS On-line antioxidant, α-amylase, α-glucosidase, pancreatic lipase, acetyl-and butyrylcholinesterase inhibition activity of Chaenomeles fruits determined by polyphenols and other chemical compounds, Antioxidants 9 (1) (2020) 60.
[31] C. Chu, et al., A novel high-resolution monophenolase/diphenolase/radical scavenging profiling for the rapid screening of natural whitening candidates from Peaonia lactiflora root and their mechanism study with molecular docking, J. Ethnopharmacol. 282 (2022), 114607.

[32] J. Song, et al., Synthesis of p-coumaroyl amino acid derivatives and evaluation of their anti-oxidative and anti-tyrosinase activities, Sustainable Chemistry and Pharmacy 29 (2022), 100752.

[33] 王立军, 白芍及桑白皮中酪氨酸酶抑制剂的筛选及其活性成分的抑制动力学研究 2016, 新建: 塔里木大学.

[34] B. Luo, *Study on a New Screening Method of Natural Tyrosinase Inhibitors Based on HPLC Post-column Derivatization [master's Thesis]*. Alaer (XJ), Tarim University, 2015.

[35] L. Mou, et al., Comparison of bovine serum albumin glycation by ribose and fructose in vitro and in vivo, Biochim. Biophys. Acta (BBA) - Mol. Basis Dis. 1868 (1) (2022), 166283.

[36] Q. Zhang, et al., Chinese bayberry (Myrica rubra) phenolics mitigated protein glycoxidation and formation of advanced glycation end-products: a mechanistic investigation, Food Chem. 361 (2021), 130102.

[37] J. Wittenauer, et al., Inhibitory effects of polyphenols from grape pomace extract on collagenase and elastase activity, Fitoterapia 101 (2015) 179–187.

[38] Z. He, W. Xia, Analysis of phenolic compounds in Chinese olive (Canarium album L.) fruit by RPHPLC–DAD–ESI–MS, Food Chem. 105 (3) (2007) 1307–1311.

[39] S. Erşan, et al., Identification of phenolic compounds in red and green pistachio (pistacia vera L.) hulls (exo- and mesocarp) by HPLC-DAD-ESI-(HR)-MSn, J. Agric. Food Chem. 64 (26) (2016) 5334–5344.

[40] I.M. Abu-Reidah, et al., HPLC–DAD–ESI-MS/MS screening of bioactive components from Rhus coriaria L. (Sumac) fruits, Food Chem. 166 (2015) 179–191.

[41] L. Dienaitė, et al., Isolation of strong antioxidants from Paeonia officinalis roots and leaves and evaluation of their bioactivities, Antioxidants 8 (8) (2019) 249.

[42] G. Zengin, et al., In vitro tyrosinase inhibitory and antioxidant potential of Consolida orientalis, Onosma isauricum and Spartium junceum from Turkey, South Afr. J. Bot. 120 (2019) 119–123.

[43] P. Xiong, et al., Identification of the tannins in traditional Chinese medicine paeoniae radix alba by UHPLC-Q-exactive orbitrap MS, Arab. J. Chem. 14 (11) (2021), 103398.

[44] S. Parker, et al., A pharmacological review of bioactive constituents of Paeonia lactiflora Pallas and Paeonia veitchii Lynch, Phytother Res. 30 (9) (2016) 1445–1473.

[45] Y.-H. Shi, et al., Characterization and quantification of monoterpenoids in different types of peony root and the related Paeonia species by liquid chromatography coupled with ion trap and time-of-flight mass spectrometry, J. Pharmaceut. Biomed. Anal. 129 (2016) 581–592.

[46] L. Zhu, et al., Comparison of chemical profiles between the root and aerial parts from three Bupleurum species based on a UHPLC-QTOF-MS metabolomics approach, BMC Compl. Alternative Med. 17 (2017) 1–12.

[47] S. Wang, et al., Composition of peony petal fatty acids and flavonoids and their effect on Caenorhabditis elegans lifespan, Plant Physiol. Biochem. 155 (2020) 1–12.

[48] R. Nie, et al., Identification and characterisation of bioactive compounds from the seed kernels and hulls of Paeonia lactiflora Pall by UPLC-QTOF-MS, Food Res. Int. 139 (2021), 109916.

[49] F.M. Rezende, et al., Acylated flavonoid Glycosides are the main Pigments that Determine the flower Colour of the Brazilian native tree Tibouchina pulchra (Cham.) Cogn, Molecules 24 (4) (2019) 718.

[50] D. Şöhretoğlu, et al., Discovery of potent α-glucosidase inhibitor flavonols: insights into mechanism of action through inhibition kinetics and docking simulations, Bioorg. Chem. 79 (2018) 257–264.

[51] I. Fecka, W. Cisowski, Tannins and flavonoids from the Erodium cicutarium herb, Z. Naturforsch. B Chem. Sci. 60 (5) (2005) 555–560.

[52] J. Chen, et al., Flavonoids isolated from the flowers of limonium bicolor and their in vitro antitumor evaluation, Phcog. Mag. 13 (50) (2017) 222–225.

[53] C. Braunberger, et al., LC-NMR, NMR, and LC-MS identification and LC-DAD quantification of flavonoids and ellagic acid derivatives in Drosera peltata, J. Chromatogr., B: Anal. Technol. Biomed. Life Sci. 932 (2013) 111–116.

[54] C.O. Lima Â, R.S. Conceição, Hydroxycinnamic acid-spermidine amides from Tetragonisca angustula honey as anti-Neospora caninum, In vitro and in silico studies 98 (6) (2021) 1104–1115.

[55] Z. Li, et al., Deep Annotation of Hydroxycinnamic Acid Amides in Plants Based on Ultra-High-Performance Liquid Chromatography-High-Resolution Mass Spectrometry and Its In Silico Database 90 (24) (2018) 14321–14330.

[56] V. Handrick, T. Vogt, A. Frolov, Profiling of hydroxycinnamic acid amides in Arabidopsis thaliana pollen by tandem mass spectrometry, Anal. Bioanal. Chem. 398 (7–8) (2010) 2789–2801.

[57] Z. Peng, et al., Synthesis, antioxidant and anti-tyrosinase activity of 1,2,4-triazole hydrazones as antibrowning agents, Food Chem. 341 (Pt 2) (2021) 128265.

[58] S.Q. Wu, et al., A fast and accurate method for the identification of peroxidase inhibitors from Radix Salvia Miltiorrhizae by on-flow biochemical assay coupled with LC/Q-TOF-MS: comparison with ultrafiltration-based affinity selection, Anal. Bioanal. Chem. 410 (18) (2018) 4311–4322.

[59] X.W. Zhang, et al., Recent advance in the discovery of tyrosinase inhibitors from natural sources via separation methods, J. Enzym. Inhib. Med. Chem. 36 (1) (2021) 2104–2117.

[60] D.Q. Li, J. Zhao, S.P. Li, High-performance liquid chromatography coupled with post-column dual-bioactivity assay for simultaneous screening of xanthine oxidase inhibitors and free radical scavengers from complex mixture, J. Chromatogr. A 1345 (2014) 50–56.

[61] J. Liu, et al., Valonea tannin: tyrosinase inhibition activity, Structural Elucidation and Insights into the Inhibition Mechanism 26 (9) (2021).

[62] Z. Ju, et al., Recent development on COX-2 inhibitors as promising anti-inflammatory agents: the past 10 years, Acta Pharm. Sin. B 12 (6) (2022) 2790–2807.

[63] J.N. Zhou, et al., New flavonoids and methylchromone isolated from the aerial parts of Baeckea frutescens and their inhibitory activities against cyclooxygenases-1 and -2, Chin. J. Nat. Med. 16 (8) (2018) 615–620.

[64] M. Antunes-Ricardo, et al., In Vivo Anti-inflammatory Effects of Isorhamnetin Glycosides Isolated from Opuntia Ficus-Indica (L.) Mill Cladodes, Industrial Crops & Products, 2015.

[65] R.J. He, et al., Structural characterization and assessment of anti-inflammatory and anti-tyrosinase activities of polyphenols from Melastoma normale, Molecules 26 (13) (2021).

[66] F.A. Qais, et al., Understanding the mechanism of non-enzymatic glycation inhibition by cinnamic acid: an in vitro interaction and molecular modelling study, RSC Adv. 6 (2016).

[67] S. Dubey, et al., Glycolytic Enzyme Inhibitory and Antiglycation Potential of Rutin, Future Journal of Pharmaceutical Sciences, 2017. S2314724515300480.

[68] C.C. Lee, B.H. Lee, Y.J. Lai, Antioxidation and antiglycation of Fagopyrum tataricum ethanol extract, J. Food Sci. Technol. 52 (2) (2015) 1110–1116.

[69] Ö. Bahadır Acıkara, et al., Inhibitory activity of Podospermum canum and its active components on collagenase, elastase and hyaluronidase enzymes, Bioorg. Chem. 93 (2019), 103330.